Nanoscale

PAPER

View Article Online
View Journal | View Issue



Cite this: *Nanoscale*, 2025, **17**, 26855

# Polydopamine-coated flat glass surfaces for nanoplastics uptake and Raman-based detection: a case study with polystyrene

Serena Schiavi,[a] Angelo Taglietti, *[a] Pietro Galinetto,[b] Benedetta Albini [b] and Om Prakash[b]

Pollution caused by nanoplastics presents great challenges for researchers because of the lack of sensitivity of traditional analytical methods, with Raman and surface-enhanced Raman spectroscopy (SERS) becoming strategic for their detection. The main drawbacks lie in the poor signals of traditional Raman spectroscopy, requiring high concentrations of analytes, and the non-homogeneous distribution often limiting reliable detection when exploiting SERS on dried samples. Herein, we propose a simple strategy based on a coating layer of polydopamine (PDA) on simple glass substrates to exploit the adhesive properties of the biopolymer for the grafting and thus evenly pre-concentration of polystyrene nanoplastics (PS-NPs), further analysed using Raman and SERS. An in-depth analysis on the role of pH in PDA adhesive properties demonstrates the importance of electrostatic interactions toward different kinds of PS-NPs, presenting different *Z*-potential values. Moreover, PS-NPs of different sizes were analysed, ranging from 1 μm down to 15 nm. Raman detection of 100 nm and 1 μm PS-NPs was achieved, demonstrating that the PDA coating layer enables NPs pre-concentration and their subsequent detection by Raman spectroscopy. The versatility of the PDA substrate was also proven by grafting gold nanostars, creating a SERS substrate capable of detecting PS-NPs down to 15 nm.

Received 4th July 2025,
Accepted 25th October 2025

DOI: 10.1039/d5nr02834e

rsc.li/nanoscale



## 1. Introduction

Pollution caused by the pervasive presence of plastic in the environment has emerged as a significant and global problem, with nanoplastics (NPs)—plastic particles smaller than 1 μm—representing a particularly significant threat.[1] This is due to a series of factors, including their high surface area, coupled with potential toxicity enhanced by bioaccumulation phenomena, as they can easily penetrate biological membranes.[2] All these factors suggest obvious risks associated with their presence in ecosystems and the human body.[3,4]

The detection of NPs in environmental matrices thus represents a formidable challenge, because traditional analytical techniques often lack the sensitivity, specificity, or resolution required for accurate identification and quantification.[5] Nevertheless, recent advances in material science and spectroscopic methods have opened up new routes to address this issue.[6]

Among all the synthetic plastic polymers, which pose a serious risk, polystyrene (PS) is surely the most representative example, as it is one of the most commonly produced plastics and thus, one of the biggest contributors to environmental pollution.[7] Beside the fact that it is not biodegradable and can persist in the environment for centuries, it can easily get fragmented into micro and nanodebris, which constitute a serious hazard for wildlife that may ingest it, especially in the marine environment, where it is ubiquitous, and its accumulation is highly significant.[8] All this, added to the potential of PS to carry harmful persistent organic pollutants,[9] makes it essential to develop user-friendly on-site methodologies able to easily monitor pollution by PS-NPs in different environments.

Raman spectroscopy, a powerful analytical technique capable of providing molecular fingerprints with high spatial resolution, offers high specificity for molecular characterization and provides a robust platform for the detection of microplastics (MPs) and, in principle, of NPs. The unique Raman scattering properties of different polymers constituting MPs and NPs allow for their precise identification and quantification even in complex environmental samples.[10]

Nevertheless, the Raman detection of NPs has some serious limitations in terms of sensitivity, as their signals can be very weak. Moreover, in general, Raman techniques suffer from diffraction limits when moving to sub-micron dimensions.[11] Thus, the fact that Raman signals are feeble strongly restricts the application of this technique to solid samples or highly concentrated aqueous solutions, often making the detection of

[a]*Dipartimento di Chimica, Università di Pavia, via Taramelli 12, 27100 Pavia, Italy. E-mail: angelo.taglietti@unipv.it*
[b]*Dipartimento di Fisica "A.Volta", Università di Pavia, via Bassi 6, 27100 Pavia, Italy*

small NPs in diluted aqueous suspensions impossible without resorting to massive and efficient preconcentration.[5]

These limitations, however, can be overcome by exploiting surface-enhanced Raman spectroscopy (SERS), a technique that significantly increases the Raman scattering signals of molecules adsorbed on rough metal surfaces or nanoparticles.[12–16] Several examples of the application of SERS to the detection of NPs have appeared in the last few years.[17] However, in most cases, the proposed methods involve preconcentration steps on the sample or rely on the drying of suspensions on the SERS-active substrate, a procedure which has intrinsic flaws, like the possibility of coffee ring effects and more generally, an uneven distribution of the analytes. Moreover, even though they have good results, most strategies so far suggested propose time-consuming preparation and complex synthetic methods.[10,17–19]

For instance, in a very recent study by Lin *et al.*,[19] a quantitative method for the detection of small NPs was optimized by exploiting hydrophobic CuO@Ag nanowire substrates combined with a multiplex-feature analysis strategy based on the coffee ring effect. Although this method enables the detection of 50 nm PS-NPs down to $10^{-10}$ wt%, the preparation of the SERS-active substrate involves many steps, namely the synthesis of CuO NWs, followed by silver deposition by thermal evaporation, further modified by means of infrared thermal radiation.

Polydopamine (PDA) is a bioinspired polymer known for its strong adhesive properties and for its ability to form stable coatings with controllable thickness on virtually any kind of inorganic or organic substrate.[20] Its universal adhesion and functionalization capabilities, mainly due to the presence of catechols and amino groups, have shown promise in enhancing the binding of molecules or molecular entities in general, even at the micro or nanoscale.[21,22] Even if only a very limited number of examples of interactions between NPs and PDA surfaces are present in the literature,[23,24] it seems obvious that the features of PDA offer a unique opportunity for the capture of NPs, thus making PDA an ideal candidate for concentrating NPs from environmental samples to allow their identification and quantification. The grafting of NPs to PDA-coated surfaces can benefit from various contributions, including π–π interactions, hydrogen bonding, and electrostatic interactions. Moreover, the use of a PDA-coated surface should, in principle, allow the co-grafting of SERS-active nanostructures and NPs.

This work explores the possibility of using PDA as a grafting and pre-concentrating substrate to bind PS-NPs, coupled with the use of Raman spectroscopy and SERS for their detection. By integrating these technologies, we demonstrate how this approach can be proposed as a reliable and efficient method for monitoring PS-NPs, present in aqueous suspension at ppm concentration, thereby contributing to broader efforts to mitigate plastic pollution and safeguard environmental health. At this proof-of-concept stage, we turned our attention to simple bidimensional flat substrates represented by glass cover slips, which are cost-effective and can be easily coated with a PDA layer, offering a practical substrate for thorough characterization.

The adhesive features of PDA are strongly dependent on the protonation/deprotonation state of its exposed functional groups and thus on the pH of the solutions in which they are immersed. Therefore, here we propose a rational study to understand the role of pH in the grafting capability of PDA surfaces, investigating the behaviour of PS-NPs functionalized with different terminal groups. To our knowledge, there are no examples in the literature reporting the exploitation of PDA-coated substrates for the capture and preconcentration of PS-NPs through pH-modulated electrostatic interactions. The dimensions of the PS-NPs also play a crucial role in their determination; thus, we extended the investigation to PS-NPs ranging from 1 μm to 15 nm. We demonstrated how the detection of large NPs grafted on the PDA surfaces can be easily achieved by standard Raman measurements. Conversely, moving to a smaller size, the versatility of the PDA layer was exploited by grafting gold nanostars (GNS) and creating a SERS substrate capable of detecting PS-NPs down to 15 nm at ppm level.

## 2. Experimental section

### 2.1. Materials

Dopamine hydrochloride (≥99%) was purchased from Thermo Scientific. Trizma base (≥99.9%), sodium citrate tribasic dihydrate (≥99.0%), Rhodamine 6G (99%), silver nitrate (≥99%), hydrochloric acid (≥37%), 2-propanol (≥99.5%), gold(III) chloride trihydrate (~30 wt% in HCl, 99.99%), sodium borohydride (98%), L-ascorbic acid (≥99%), 2-[4-(2,4,4-trimethylpentan-2-yl) phenoxy]-ethanol (Triton X-100), polystyrene latex beads, (1 μm size, plain), and polystyrene latex beads, (100 nm size, plain) were purchased from Sigma-Aldrich. Polystyrene latex beads (surface $SO_3H$, size 100 nm) and polystyrene latex beads (surface $NR_3^+$, size 100 nm) were purchased from micromod Partikeltechnologie GmbH. Polystyrene latex beads (15 nm, plain) were purchased from D.B.A. Italia s.r.l. PMMA nanoparticles (120 nm) were purchased from KF Technology Srl and microscopy glass cover slips 21 mm × 26 mm were purchased from Carlo Erba. Water was deionized and double distilled ($ddH_2O$).

### 2.2. Characterization

UV-vis-NIR absorption spectra of colloidal suspensions were acquired with a Cary 60 spectrophotometer in the 300–1100 nm range.

*Z*-Potential measurements were performed on 1 mL colloidal suspension with a Zetasizer Nano-ZS90 (source: polarized He–Ne laser, 30 mW output power, vertically polarized) with a capillary cell.

Surface zeta potential (SZP) measurements were performed on a glass-based substrate employing a surface zeta potential kit from Malvern on a Zetasizer Nano-ZS90. The samples were fixed on a specific sample holder capable of regulating its position with respect to the laser beam. Measurements were performed following the manufacturer's instructions, dipping the

 

sample holder in a suspension of positively or negatively charged polystyrene standard nanoparticles as tracer materials.

Transmission electron microscopy images were collected on a Jeol JEM-1200 EX II instrument. 10 μL of samples were dropped and left to dry overnight on copper grids, 300 mesh, coated with Collodion solution.

Raman and SERS measurements were performed at room temperature using an XploRa Plus (HORIBA Scientific) integrated confocal spectrometer equipped with an Olympus BX43 microscope with a motorized *xy* stage, acting as a sample holder. The spectral resolution was about 3 $cm^{-1}$, and the light signals were revealed by an Open Electrode CCD camera cooled down to −60 °C in a multistage Peltier air-cooling system. 532 nm and 638 nm laser light (90 mW) were used as excitation sources. Neutral filters with different optical densities were used to set the proper incident laser power.

Scanning electron microscopy (SEM) images were acquired with a Tescan Mira XMU variable pressure field emission scanning electron microscope–FEG SEM (Tescan USA Inc., Warrendale, PA, USA), located at the Arvedi Laboratory, CISRiC, Pavia. Slides were mounted onto aluminium stubs using double-sided carbon adhesive tape and then were made electrically conductive by coating them with a thin layer of Pt/Pd (nm) in a vacuum. Images were obtained at 20 and 25 kV using an In-Beam Secondary electron detector to achieve higher spatial resolution.

### 2.3. Preparation and characterization of glass@PDA substrates

Before use, glass cover slips were first cleaned twice with *i*-propanol and once with $ddH_2O$ under sonication, 5 minutes for each cleaning step. Once cleaned, the glass slides were put in a staining jar and completely covered with 40 mL of a 2 mg $mL^{-1}$ solution of dopamine in 10 mM Tris-HCl buffer (pH 8.5) to initiate the polymerization process. After 60 min, the solution was removed, and the glasses were washed a couple of times with $ddH_2O$ and finally dried under nitrogen flux before UV-vis-NIR and SZP characterization.

### 2.4. SEM imaging following plastic uptake experiments with glass@PDA substrates

**2.4.1. pH and surface charge effect.** To assess the importance of the experimental conditions for nanoplastic uptake, *i.e.* the pH of the samples, a first series of experiments was conducted employing PS-NPs with different surface modifications. 100 nm diameter plain, $SO_3H$-functionalized and $NR_3^+$-functionalized PS-NPs were investigated as test substrates. Briefly, for each NPs uptake experiment, a glass@PDA substrate was immersed overnight in a 10 ppm suspension of plastics in 10 mM sodium citrate and then pH was adjusted with the microaddition of 1 M solutions of hydrochloric acid or sodium hydroxide. For each surface-modified sample of NPs, two different pH conditions were tested: a pH value of 3, where the glass@PDA substrate should express an overall positive surface charge, and a pH value of 6, where the glass@PDA substrate should express a negative surface charge. The results were monitored by SEM imaging.

**2.4.2. Immersion time and NPs concentration.** After we had assessed the best conditions for NPs uptake, further experiments were conducted on plain PS nanoparticles to follow both the loading kinetics and the grafting efficiency by changing the concentration of PS nanoparticles.

To follow the timescale of loading, SEM images were acquired after 1 h, 2 h 30, 4 h and 24 h of immersion of the glass@PDA substrate in 60 mL of the 10 ppm suspension of 100 nm PS-NPs at pH 3.

Setting 24 h as the optimal immersion time, four different concentrations of PS suspension were employed to investigate the rate of uptake at pH 3. Briefly, 2 ppm, 5 ppm, 10 ppm and 20 ppm suspensions of NPs were investigated through SEM imaging.

**2.4.3. Plastic uptake experiments investigating different NPs dimensions.** PS-NPs uptake experiments were performed to investigate different NPs dimensions. For 1 μm PS-NPs, 10 ppm, 20 ppm, 50 ppm and 100 ppm concentrations were analysed, keeping the optimized conditions fixed for the uptake, *i.e.* 24 h immersion at pH 3. As proof of concept, an uptake experiment for 15 nm PS-NPs was performed with 10 ppm concentration, again keeping fixed the conditions 24 h of immersion at pH 3.

### 2.5. Raman detection of PS-NPs loaded on glass@PDA

Raman measurements were performed directly on dry glass@PDA substrates loaded with 100 nm and 1 μm PS-NPs. Raman spectra were collected with a 532 nm laser source, 100× magnification objective, 106 W $cm^{-2}$ nominal power density, with an exposure of 30 s and 10 accumulations. Each substrate was investigated by mapping a total area of 225 $\mu m^2$ and sampling every 1.5 μm. The main Raman modes of polystyrene are reported in Table S1.[25,26]

### 2.6. Synthesis of gold nanostars (GNS) and preparation of glass@PDA@GNS SERS substrate

GNS were prepared following a well-established seed-growth approach.[27] First, gold seeds were prepared by adding, in the following order, 5 mL of a 0.2 M aqueous solution of Triton-X-100, 5 mL of a $4.5 \times 10^{-4}$ M aqueous solution of $HAuCl_4$ and then rapidly adding 600 μL of a 0.01 M solution of $NaBH_4$. The seeds thus obtained show an orange-brownish colour and were stored in an iced bath prior to use (within a couple of hours). The growth step was achieved as follows: 2.5 mL of a 0.004 M solution of $AgNO_3$ and 50 mL of a $4.5 \times 10^{-4}$ M solution of $HAuCl_4$ were added in this order to 50 mL of a 0.2 M solution of Triton-X-100 under stirring. Then, rapidly and in this order, 1.7 mL of a 0.0788 M solution of L-ascorbic acid and 120 μL of the seeds (just synthesised) were added. After the last addition, the suspension turned from light pink to a dark blue/grey colour, and the suspension was kept under stirring for 15 min before characterization.

The glass@PDA substrates were then functionalized with the GNS synthesised as described above. Briefly, glass@PDA

substrates were immersed in a colloidal suspension of GNS in 5 mM citric acid aqueous solution overnight. Then the colloid was removed, the obtained glass@PDA@GNS were washed three times with $ddH_2O$ and finally dried under nitrogen flux before characterization.

### 2.7. SERS performance of glass@PDA@GNS substrates

The SERS response of glass@PDA@GNS was tested using Rhodamine 6G (R6G), a well-known Raman reporter, as a probe molecule. Briefly, 80 μL of a 10 μM aqueous solution of R6G was deposited on the SERS substrates and covered with a clean glass cover slip. The SERS measurements were performed immediately after the deposition to keep the solution wet using a 638 nm laser source, 50× magnification objective, 106 W $cm^{-2}$ nominal power density, with an exposure of 10 s and 5 accumulations. On each substrate tested, 10 different areas were sampled. The main Raman modes of R6G are reported in Table S2.[28,29]

### 2.8. SERS measurements of 15 nm NPs

SERS measurements were performed directly on dry glass@PDA@GNS substrates loaded with 15 nm PS-NPs. SERS spectra were collected with a 638 nm laser source, 100× magnification objective, 106 W $cm^{-2}$ nominal power density, with an exposure of 10 s and 10 accumulations. Each substrate was investigated by mapping a total area of 225 $\mu m^2$, sampling every 1.5 μm.

## 3. Results and discussion

### 3.1. Preparation and characterization of glass@PDA substrate

The coating of glass cover slips with a thin layer of PDA was performed by following a simple and well-known dip-coating procedure, described by Lee *et al.*[20] Briefly, after a cleaning step described in section 2.3., cleaned glass cover slips were immersed in a 2 mg $mL^{-1}$ solution of dopamine in 10 mM Tris buffer (pH 8.5), resulting in the deposition of a PDA film after 1 h. To stop the self-polymerization process, the solution was removed, and the PDA-coated cover slips were washed a couple of times with $ddH_2O$ and dried under nitrogen flux.

This route allows the glass slides to be coated with a nanometric layer of the polymer. In more detail, with these experimental conditions, the thickness of the deposited PDA layer could be estimated to be less than 10 nm.[30,31] A representative UV-vis spectrum of a PDA-coated slide glass (glass@PDA) is reported in Fig. S1.

In order to understand the influence of pH on the grafting properties of PDA, surface zeta potential measurements of glass@PDA substrates at different pH values were performed. As already confirmed by other studies,[32–34] the PDA surface can exhibit a switch from a positive to a negative surface charge, moving from pH values lower than 4 to higher pH values. This is due to the protonation and deprotonation equilibria that involve the catechols and amino groups. For the purpose of this work, we were interested only in analysing the two extreme conditions for plastic uptake; thus, all the experiments aimed at understanding the role of the surface charge of PDA on its adhesive capabilities were performed at pH values of 3 and 6, where the polymer should express the two different charges.

By means of DLS, as described in section 2.2., it was possible to measure the SZP of the glass@PDA surface when immersed in two different buffered solutions at different pH, of 3 and 6. From the measurements, it was possible to obtain a value of 17 ± 2 mV at pH 3.12 and a value of −35 ± 2 mV at pH 6.00. It must be stressed that the decision to perform all the experiments by selecting pH 3 and 6 as the extremes was taken after SZP titration of the glass@PDA surface (the full set of data is reported in Table S3).

What can be observed from the experimental results of SZP is reported in the scheme represented in Fig. 1. The peculiar feature of PDA films, of displaying different surface charges depending on the pH of the media, not only suggests the importance of electrostatic interactions for NPs adhesion, but it also tells us that by properly modulating the pH, it is possible to load both negative and positive objects.

### 3.2. Uptake of PS-NPs with glass@PDA substrates: SEM imaging studies

**3.2.1. The role of pH on surface charge and the effects on NPs uptake.** The first rounds of experiments performed on glass@PDA samples were devoted to demonstrate the pivotal importance of pH in NPs uptake. To assess this, we decided to employ different kinds of PS-based NPs with a fixed diameter of 100 nm but with different surface modifications: plain PS-NPs, $SO_3H$-functionalized PS-NPs (PS-$SO_3H$-NPs) and $NR_3^+$-functionalized PS-NPs (PS-$NR_3^+$-NPs). The intent was to evaluate grafting efficiency as a function of electrostatic interactions: negatively charged particles should benefit attraction from a positively charged PDA surface (pH < 4) while undergoing repulsion from negative PDA surfaces (pH > 4); clearly, the opposite behaviour is expected from positively charged particles. The *Z*-potentials of all PS-NPs employed are reported in Table 1, measured at the chosen pH values.

The NPs loading experiments were conducted by dipping each glass@PDA in 60 mL of 100 nm NPs colloidal suspension at 10 ppm concentration for 24 h. Six different experiments were performed, one for each of the PS-NPs mentioned above, at two different pH conditions, when the PDA displays a positive surface charge (pH 3) and a negative surface charge (pH 6). After 24 h of immersion, each sample was accurately washed with $ddH_2O$ water and dried under nitrogen flux before characterization. Fig. 2 shows representative SEM images acquired for each loading experiment.

As expected, the best grafting efficiency is achieved when attractive electrostatic interactions between PS-NPs and the PDA surface can be established, while, as can be observed from the SEM images, even in repulsive regimen, some NPs can still be grafted on the substrate. This behavior can be ascribed to other weak interactions that PDA can establish.[35] The layer of PS-NPs observed in attractive conditions appears quite homogeneous and complete, reflecting a situation in

 

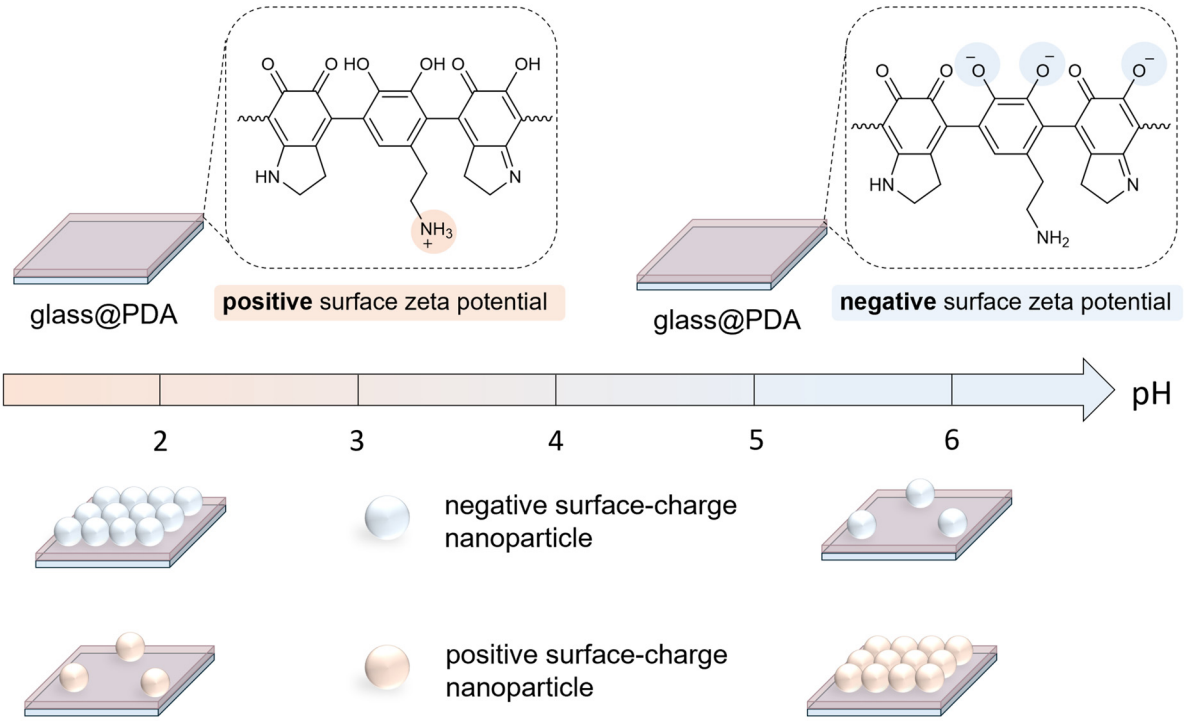


**Fig. 1** Schematic illustration of the expected behaviour of a PDA surface towards nanoplastics with positive (reddish) or negative (light blue) *Z*-potential values.

**Table 1** *Z*-Potential values of different PS-NPs employed, in different pH conditions

| PS-NPs | *Z*-Potential (mV) at pH 3 | *Z*-Potential (mV) at pH 6 |
|---|---|---|
| PS-$SO_3H$-NPs | −51 ± 3 | −47 ± 2 |
| PS-$NR_3^+$-NPs | 36 ± 3 | 25 ± 4 |
| PS-plain-NPs | −35 ± 2 | −45 ± 4 |

which all the surface can be covered with the NPs present in suspension. Some aggregates of nano-objects are observed, but with limited vertical overlap of a few individuals. Indeed, these findings carry an important piece of information: to properly capture NPs with PDA-coated substrates, the relationship between the *Z*-potential of the NPs and the surface charge of PDA must be optimized, which can be easily obtained by regulating the pH of aqueous samples of PS-NPs.

**3.2.2. Investigation of loading timescale and NPs concentration.** The timescale required to achieve optimal grafting under favourable conditions was also investigated. We performed SEM imaging on glass@PDA samples after different immersion times in a 100 nm diameter plain PS-NPs suspension at a 10 ppm concentration. As can be observed in Fig. S2, under these concentration conditions, almost complete surface coverage is obtained after 2.30 h, while the maximum uptake is achieved after 24 h of immersion, as can also be seen from the calculated number of nanoparticles taken up. This behavior was also confirmed by the Raman experiments discussed in more detail in section 3.3. For this reason, all further uptake experiments were performed by fixing 24 h as the standard immersion time.

Once the experimental conditions for correct uptake had been set, we investigated the effect of the concentration of PS-NPs to gain a rough idea of the capture efficiency of the flat PDA surfaces. Fig. 3 shows SEM images obtained after 24 h of immersion of a glass@PDA substrate in 60 mL of suspensions of plain PS-NPs at various concentrations, *i.e.* 20 ppm, 10 ppm, 5 ppm and 2 ppm. As could have been foreseen, it can clearly be observed how the number of NPs captured by the surface increases as the PS concentration increases.

While a linear trend for the increase in the number of NPs grafted per unit area can be observed up to 10 ppm, increasing the concentration beyond that no longer results in a significant increase in the quantity of grafted NPs, as the surface appears to be already saturated at 10 ppm. These preliminary experiments conducted with the as-proposed flat PDA substrate show a semi-quantitative method for monitoring PS-NPs at low concentrations, highlighting the great potential of this simple and fast technique.

**3.2.3. Investigation of plastic uptake with different NPs dimensions.** As proof of concept of the as-proposed methodology, we tested the uptake capability of the glass@PDA substrate for NPs of different dimensions, ranging from 15 nm to 1 μm, considering this as the upper limit for the proper definition of NPs. Having already established the best experimental conditions to optimize the grafting procedure and con-

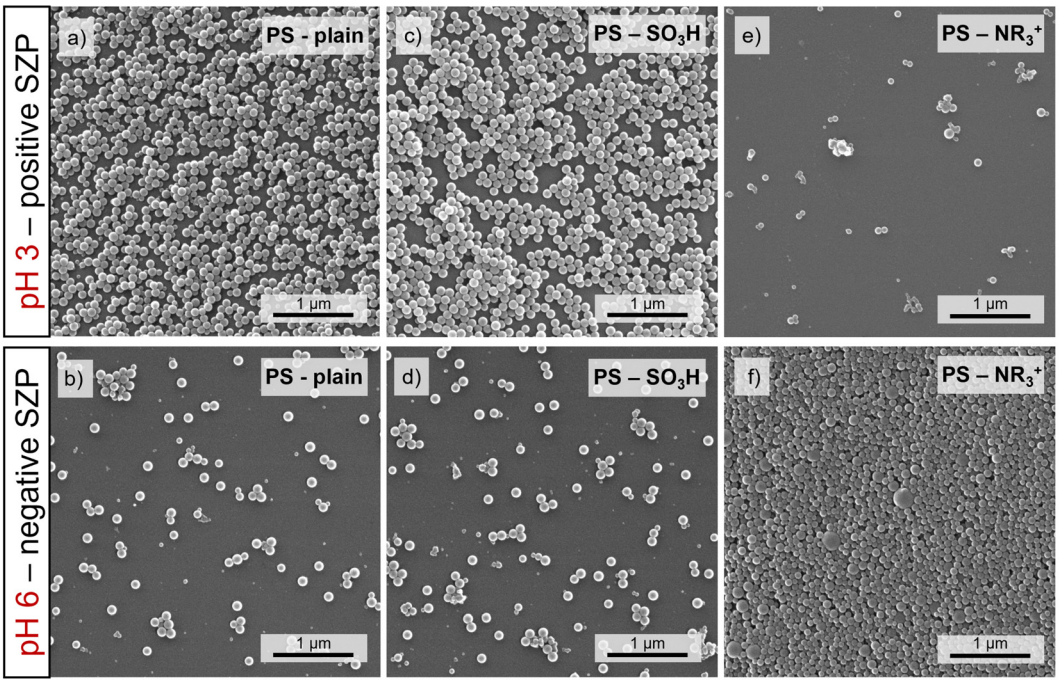


**Fig. 2** Representative SEM images of glass@PDA samples immersed in 60 mL of 10 ppm water suspension of: (a) plain PS-NPs at pH 3; (b) plain PS-NPs at pH 6; (c) PS-$SO_3H$-NPs at pH 3; (d) PS-$SO_3H$-NPs at pH 6; (e) PS-$NR_3^+$-NPs at pH 3; (f) PS-$NR_3^+$-NPs at pH 6.

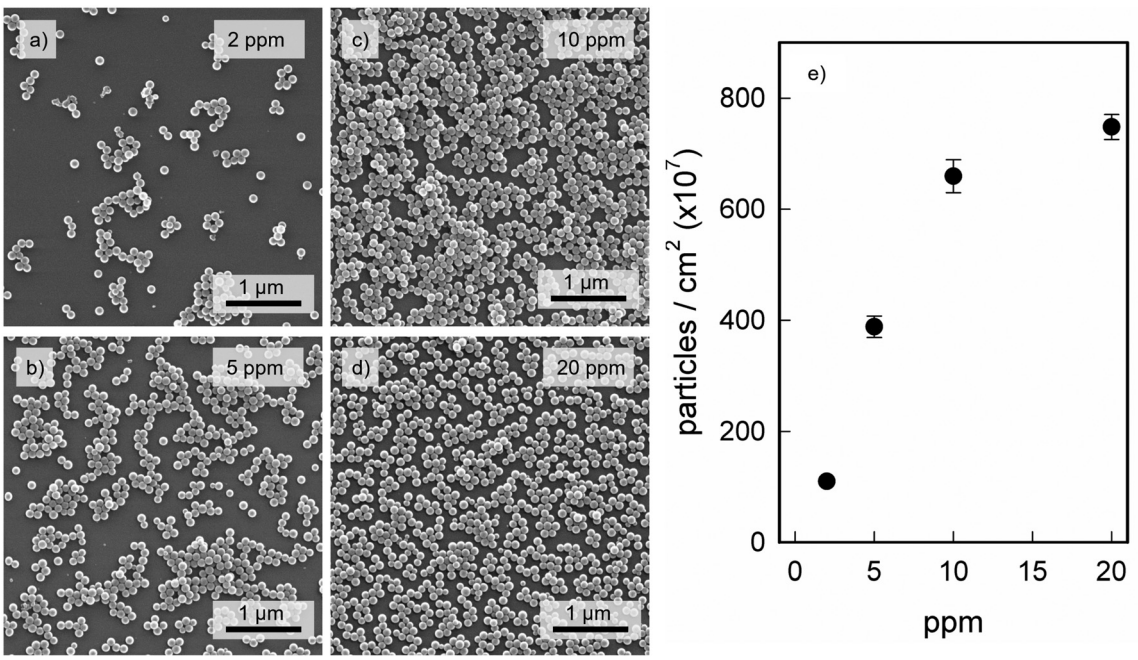


**Fig. 3** Representative SEM images of glass@PDA samples immersed in 60 mL of aqueous suspensions of 100 nm diameter plain PS-NPs at pH 3 with concentrations of (a) 20 ppm; (b) 10 ppm; (c) 5 ppm; (d) 2 ppm. (e) Number of particles per unit area obtained from SEM images as a function of NPs-PS concentration in suspension averaged from three different SEM images.

sidering that we again selected plain PS-NPs (which display a negative charge over the whole investigated pH range, as reported in Table 1), we performed the uptake experiments by setting the pH at a value of around 3.

The uptake experiments using 1 µm size PS-NPs were performed at concentrations of 10 ppm, 20 ppm, 50 ppm and 100 ppm, following the same procedure described for the 100 nm PS-NPs (section 3.2.2.). Representative SEM

 

images for the four different uptake experiments are shown in Fig. 4.

It is worth noting that the SEM images obtained with 1 μm PS-NPs show a less dense layer of grafted PS particles than that obtained for the 100 nm PS-NPs. This is particularly evident when comparing the glass@PDA substrate grafted with 10 ppm of 100 nm PS with the substrate coated with 1 μm PS at the same concentration. The reason is obvious: when the concentration expressed in mass units (ppm) is kept constant, an increase in diameter is reflected in a reduction of the number of objects. This clearly explains why, even with an NPs concentration of 100 ppm, the glass@PDA still does not show a homogeneous and complete coverage of the substrate with 1 μm PS.

Either way, when the concentration is increased, the number of 1 μm PS-NPs grafted on glass@PDA evidently increases, confirming again the capability of PDA surfaces as a tool able to operate quite efficient pre-concentration, which could be useful for detection and removal of NPs from aqueous samples.

A similar grafting experiment was conducted on 15 nm diameter PS-NPs at 10 ppm concentration. It was confirmed again (as depicted in Fig. S3) that working at acidic pH values, and thus, with a positive PDA surface charge, enables pre-concentration on the glass@PDA surface PS-NPs. From the SEM images, some aggregates can clearly be observed, appearing as fused objects because of Pt metallization. This, summed up to the SEM limit resolution, made it almost impossible to perform quantitative analysis of the number of grafted objects, even though we could still observe complete coverage of the PDA surface with the 15 nm PS-NPs. To address the resolution issue, the same PDA-coating approach was applied on silicon wafers instead of glass to perform imaging with better resolution, avoiding the use of Pt sputtering, which can significantly affect resolution when working with small nano-objects. Indeed, to improve imaging quality, we performed the pre-concentration of 15 nm PS-NPs using a 2.5 ppm suspension (SEM images are shown in Fig. S4).

Overall, this imaging study demonstrates that a simple PDA-coated flat surface can efficiently adsorb PS-NPs, and that the system performs effectively with both positively and negatively charged NPs by simply adjusting the pH of the sourronding medium. On top of that, the pre-concentration of PS-NPs was also investigated in terms of dimensional range, proving to work with NPs ranging from 1 μm to 15 nm in diameter by simple immersion of the PDA substrates in the samples spiked with PS-NPs at ppm level.

After thoroughly demonstrating the role of pH on the expression of PDA interactions, we wanted to confirm that the NPs preconcentrating strategy can be exclusively attributed to the presence of PDA itself. Thus, as control experiments, bare glass cover slips were immersed in 10 ppm and 100 ppm water suspension of 100 nm and 1 μm PS-NPs at pH 3. As expected, without the PDA-coating layer, PS-NPs did not interact with the substrates, as evident from the SEM images reported in Fig. S5, confirming once again the key role of the biopolymer.

### 3.3. Raman detection of pre-concentrated PS-NPs

Having assessed by SEM imaging the best conditions for effective uptake of PS-NPs with the proposed PDA-based substrate, we attempted to use Raman spectroscopy for their actualdetection and identification. The purpose was to demon-

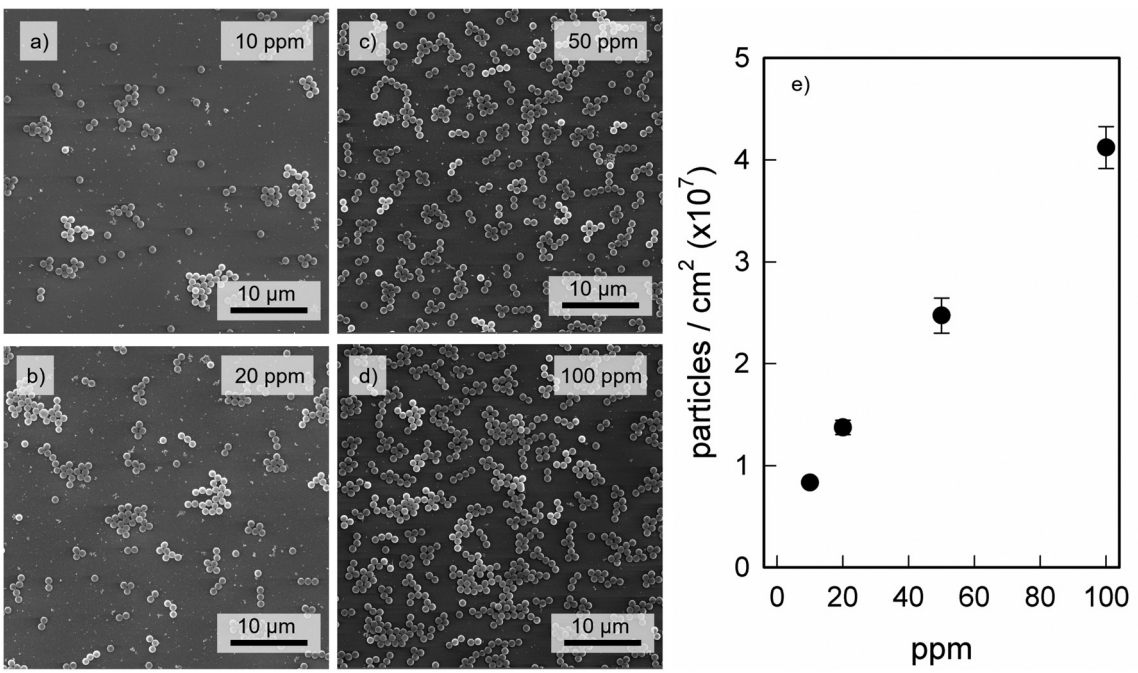


Fig. 4 Representative SEM images of glass@PDA samples immersed in 60 mL water suspension of 1 μm diameter plain PS-NPs at pH 3 at concentrations (a) 10 ppm; (b) 20 ppm; (c) 50 ppm; (d) 100 ppm; (e) the number of particles per unit area obtained from SEM images, as a function of NPs-PS concentration in suspension averaged from three different SEM images.

strate, by exploiting the grafting capability of PDA substrates, how PS-NPs are pre-concentrated and thus easily detected by means of traditional Raman spectroscopy, even at the nanoscale.

Raman measurements were performed on the PDA substrates loaded with PS-NPs, analysed in section 3.2. First, 1 μm PS-NPs samples were analysed. Fig. 5a shows the average Raman spectra of glass@PDA substrates loaded respectively from top to bottom with 100 ppm, 50 ppm, 20 ppm and 10 ppm 1 μm PS-NPs collected as described in section 2.5. Briefly, in order to achieve reliable information related to the NPs concentration, a 225 $\mu m^2$ area was mapped with a 532 nm laser source and a 100× objective, sampling every 1.5 μm. The spectra reported in Fig. 5a were obtained by averaging all the spectra collected in the map. As can clearly be observed, the PS Raman signals increase with an increase in PS-NPs concentration. This behaviour can be followed from Fig. 5b, where the Raman intensity values of the PS characteristic peak at 1001 $cm^{-1}$ (relative to ring breathing mode)[25] are plotted as a function of concentration (red diamonds), in good agreement with the number of PS-NPs loaded per unit area as a function of their concentration (black circles). These results stress the fact that for 1 μm size NPs, which represent the upper limit of the definition of NPs based on dimensions, the exploitation of a nanometric PDA layer coupled with Raman spectroscopy can easily reveal and quantify PS-NPs.

To demonstrate the potential implementation of the PDA preconcentration method in real environmental matrices, we performed additional experiments on PS-NPs spiked into real water samples (*i.e.*, tap water and river water from the Roggia Vernavola, Pavia, Italy). In brief, 60 mL of water was spiked with 1 μm PS-NPs at a final concentration of 10 ppm, and glass@PDA substrates were immersed in the suspension for 24 h prior to Raman measurements. Raman spectra collected on precontracted PS-NPs are reported in Fig. S6. As can be observed from the Raman spectra, despite a decrease in signal intensity, the presence of PS-NPs can still be clearly identified, without any signal interference, thus confirming the effectiveness of the preconcentration strategy even in complex matrices.

Similar behavior to that discussed for 1 μm PS-NPs was observed when moving to 100 nm size PS-NPs (Fig. 6a). Here, a much weaker Raman signal is observed, as expected, as the mass of NPs brought onto the flat surfaces strongly reduces as the dimension of the NPs decreases. This result should not be surprising. It is well known that the exploitation of Raman and SERS techniques for the quantification of NPs is limited due to the aforementioned size-dependent intensities of Raman signals.[36] Nevertheless, following the intensity trend of the 1001 $cm^{-1}$ peak as a function of NPs concentration (red diamonds in Fig. 6b), we again found a good match when compared with the number of particles bound per unit area as a function of their concentration in water suspension.

To further confirm that without this PDA-based preconcentration step, the direct Raman detection of 100 nm and 1 μm PS-NPs is hindered, control experiments were conducted. Accordingly, Raman spectra were acquired from a 10 ppm aqueous suspension of 100 nm PS-NPs and a 100 ppm aqueous suspension of 1 μm PS-NPs, and the results were compared with the signals obtained from the respective concentrations of NPs preconcentrated on glass@PDA substrates. As can clearly be observed from the spectra reported in Fig. S7 and S8, the preconcentration step exploiting the adhesive properties of glass@PDA substrates is mandatory to achieve the Raman detection of NPs. Moreover, Raman investigation was also conducted on the substrates already characterized in section 3.2.1., as proof of concept for the influence of pH on the grafting procedure. As expected, no Raman signal could be

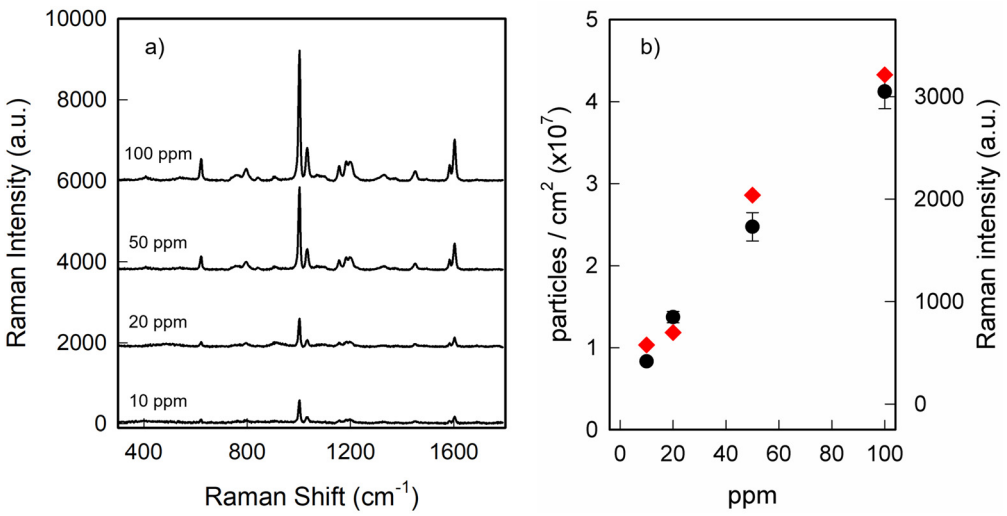


**Fig. 5** (a) Average Raman spectra obtained on glass@PDA samples after immersion in 60 mL water suspensions of 1 μm diameter plain PS-NPs at pH 3 at concentrations ranging between 10 ppm and 100 ppm; (b) intensity of 1001 $cm^{-1}$ peak as a function of concentration (red diamonds) superimposed on the number of PS particles per unit area obtained from SEM images, as a function of PS-NPs concentration in suspension (black circles).

 

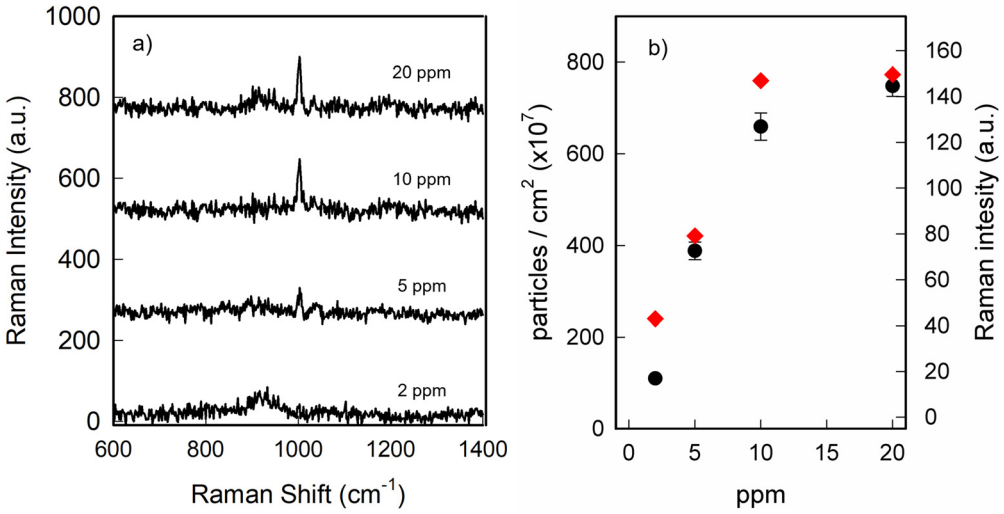


**Fig. 6** (a) Average Raman spectra obtained on glass@PDA samples after immersion in 60 mL water suspensions of 100 nm diameter plain PS-NPs at pH 3 at concentrations ranging between 2 and 10 ppm; (b) intensity of 1001 $cm^{-1}$ peak as a function of concentration (red diamonds) superimposed on the number of particles per unit area obtained from SEM images, as a function of NPs-PS concentration in suspension (black circles).

detected from the glass@PDA substrate exposed to a 10 ppm suspension of 100 nm NPs at pH 6 (see Fig. 2b). The same result was achieved with the glass@PDA substrate immersed in a 10 ppm colloidal suspension of positive PS-$NR_3^+$-NPs at pH 3 (Fig. 2e). These outcomes again highlight the fundamental role of PDA surface charge and thus the electrostatic interaction that can be established with PS-NPs. Although with just mild pH modulation, PDA can easily modify its overall surface charge, enabling an attractive interaction with the desired target to be established. Indeed, glass@PDA samples immersed in a 10 ppm suspension of PS-$NR_3^+$-NPs at pH 6 gave a neat peak around 1001 $cm^{-1}$ (Fig. S9, again obtained by averaging the spectra collected by mapping a 225 $\mu m^2$ area).

To provide confirmation that the maximum uptake of PS-NPs was achieved after 24 h, Raman measurements were performed on glass@PDA substrates immersed for different amounts of time in a 10 ppm suspension of 100 nm PS-NPs (Fig. S10). As expected, the maximum signal was obtained after 24 h of uptake, confirming what had already been observed in the SEM images shown in Fig. S2.

Lastly, to prove the applicability of PDA adhesive layers on glass supports for different nanoplastics, we decided to investigate the behavior with 120 nm PMMA NPs. After having assessed that even PMMA NPs display a negative *Z*-potential at the chosen pH values (*i.e.* −47 ± 3 mV at pH 6 and −22 ± 2 mV at pH 3), glass@PDA substrates were immersed in a 10 ppm suspension of PMMA NPs at both pH 3 and 6. As can be observed from Fig. S11, efficient preconcentration of these NPs was again achieved at pH 3, where the PDA layer could best establish favorable electrostatic interactions with the target analyte. However, although the preconcentration step was successful, Raman analysis failed to detect PMMA NPs on the glass@PDA substrate. This was not surprising, as the scattering cross-section of PMMA is significantly lower than that of PS;[37,38] therefore, Raman analysis was limited in the case of small PMMA NPs, highlighting the need for more sensitive detection strategies in such systems.

### 3.4. SERS detection of 15 nm PS-NPs

The same approach as that described above for NPs pre-concentration on glass@PDA substrates, and thus their Raman detection, was also attempted for 15 nm diameter PS-NPs. After having demonstrated the importance of the dimensions of PS-NPs on the Raman response, we were not surprised by the complete absence of any Raman signals for the smaller PS-NPs investigated. As already observed in Fig. S3, after the immersion of a glass@PDA substrate in a 10 ppm aqueous suspension of 15 nm PS-NPs at pH 3, a full and compact layer of NPs is obtained, but it seems clear that there is not enough mass of PS material pre-concentrated on the PDA surface to enable direct Raman detection. This result set the lower limit of the dimension of PS-NPs that can be successfully detected by means of simple Raman spectroscopy.

To address this issue, we chose to use the glass@PDA substrate to graft noble metal nano-objects onto its surface, before employing it for the pre-concentration of small PS-NPs. In this way, pre-concentration brings the NPs into proximity with the metal nano-objects, thereby enhancing their intrinsically weak Raman signals.

To assess this, we decided to decorate a glass@PDA substrate with gold nanostars (GNS). GNS were previously recognized as efficient SERS substrates, due to their peculiar morphologies: branches and tips guarantee the presence of hot spots and the 'lightning rod' effect.[39–42] GNS were thus synthetized according to the seed-growth procedure described in section 2.6.[27] Representative TEM images of GNS nanoparticles are reported in Fig. S12 and a UV-vis-NIR spectrum is reported in Fig. S13. The spectra show the expected plasmonic

feature close to 900 nm, which is due to the longitudinal resonance along one single branch of GNS. A second band is located around 1500 nm and is due to longitudinal LSPR involving a couple of collinear branches (not shown in this spectrum).[13] These two LSPRs are responsible for generating local field enhancement, mainly corresponding to the tips of GNS and along their main axis, as confirmed by theoretical field simulations conducted in our previous work.[43] The local field enhancement generated by these anisotropic structures is known to give strong SERS signals according to the so-called lightning rod or antenna effect.[44]

Again, the peculiar adhesive properties of PDA match well with the GNS features, as at pH 3, GNS possess a weakly negative *Z*-potential, resulting in −13 ± 2 mV. Thus, GNS grafting on the glass@PDA surface was easily achieved by immersing the PDA substrate overnight in the GNS colloidal suspension, with the pH adjusted to 3. The substrates thus obtained (glass@PDA@GNS) were then cleaned three times with dd$H_2O$ to remove all residual Triton and finally dried under nitrogen flux before characterization. Fig. S14 shows SEM images of a typical glass@PDA@GNS sample, while Fig. S15 shows a representative UV-vis-NIR spectrum of the substrate. One can observe a sensible redshift of the LSPR representative peak compared to the colloidal GNS spectrum (Fig. S13). This is due to a change in the refractive index when moving from $H_2O$ to the air/PDA interface and is probably also influenced by conjugation of plasmonic features between proximal GNS.

The SERS enhancing capability of glass@PDA@GNS substrates was tested using Rhodamine-6G (R6G) as a probe molecule following the procedure described in detail in section 2.7. An average EF of $2 \times 10^6$ was obtained using the formula reported in the SI (S16) from our previous work,[45] consistent with those previously reported in another of our studies on the same GNS prepared with a different substrate.[13]

To better visualize the SERS enhancement, Fig. S17 shows a comparison between the SERS spectrum of $10^{-5}$ M R6G solution and the corresponding Raman spectrum obtained from a $10^{-3}$ M solution of R6G.

Moreover, the reproducibility and homogeneity of the glass@PDA@GNS substrates were assessed by analyzing three independent samples, with ten different areas measured per sample. Fig. S18a shows the SERS spectra of R6G acquired from ten positions on a single substrate, confirming its good homogeneity (RSD = 5.4%). Fig. S18b reports instead the average SERS response from the three substrates, demonstrating the high reproducibility of the SERS-active substrate fabrication (RSD = 3.2%).

Lastly, the stability of glass@PDA@GNS substrates was monitored over 25 days by UV-visible spectroscopy. As shown in Fig. S19, no detectable variation in the LSPR extinction of the GNS-grafted substrates was observed, confirming their long-term stability under the tested conditions, namely simple storage in air without any special precautions.

In order to proceed with the SERS detection of PS-NPs, the glass@PDA@GNS samples were immersed overnight in aqueous suspensions of 15 nm PS-NPs at pH 3, ranging from 1 to 10 ppm. Representative SEM images of glass@PDA@GNS substrate immersed in a suspension of 15 nm PS-NPs are reported in Fig. S20 and S21. From the SEM images, the adhesion of several PS-NPs could be observed both on the surface of PDA, in the "free" space between GNS individuals and, apparently, also directly on GNS branches. This fact can be explained by the presence on GNS surfaces of the surfactant Triton X-100, which could provide some hydrophobic inter-

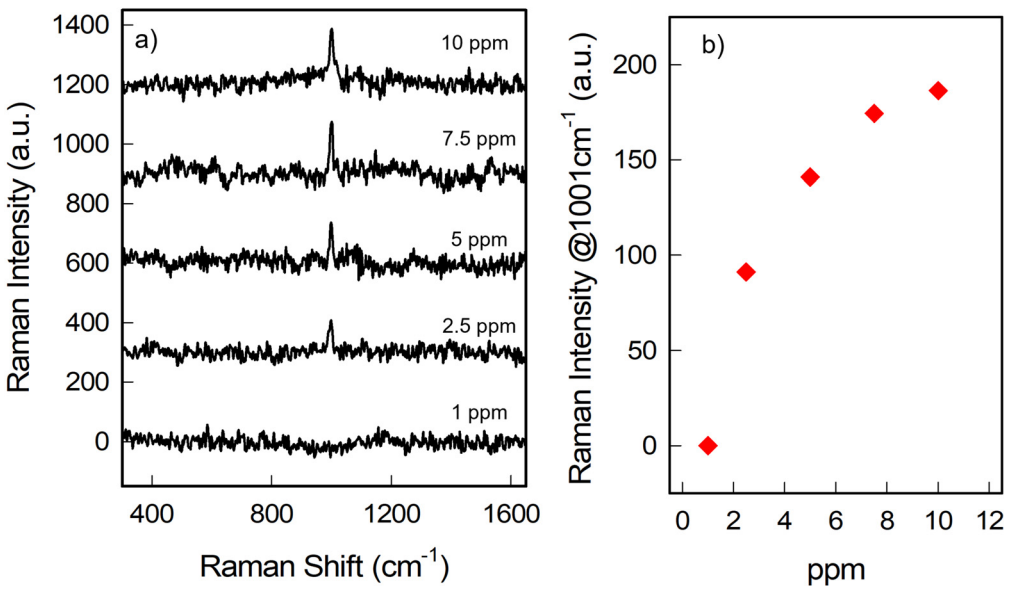


**Fig. 7** (a) Average SERS spectra obtained on glass@PDA@GNS samples after immersion in 60 mL water suspensions of 15 nm PS-NPs at pH 3 between 1 and 10 ppm; (b) intensity of 1001 $cm^{-1}$ peak as a function of concentration of 15 nm PS-NPs.

 

Table 2 Recent Raman SERS-based detection methods for micro and nanoplastics

| Substrate | PS-NPs dimension investigated | LOD | Sample treatment and detection strategy |
|---|---|---|---|
| Gold spattered on glass substrate[36] | 100–800 nm | ~0.1 mg $L^{-1}$ | Drying of aqueous NPs suspension, redispersion in organic solvent and SERS detection on coffee ring after dry dropping |
| Klarite[1] | 360 nm to 5 μm | Not calculated | Dry dropping of NPs aqueous suspension prior to Raman measurements |
| Silver nanoparticles[46] | 100 nm, 500 nm, 10 μm | 40 mg $L^{-1}$ | Aggregation of silver nanoparticles in NPs suspension prior to SERS detection |
| Elliptical gold nanoparticles[47] | 350 nm, 1 μm, 4 μm | 6.25 mg $L^{-1}$ | Aggregation of gold nanoparticles in NPs suspension and dry dropping prior to SERS detection |
| Gold nanoparticles on glass[48] | 161 nm, 33 nm, 62 nm | ~10 mg $L^{-1}$ | Dry dropping of NPs suspension prior to SERS detection |
| Silver nanoparticles[49] | 20 nm | 10–5 mg $L^{-1}$ | Self-assembly of AgNPs and nanoplastics at the ethyl acetate-PMMA/water interface. Transfer of AgNPs@PMMA film onto aluminum sheet prior to SERS measurement |
| glass@PDA and glass@PDA@GNS (this work) | 15 nm, 100 nm, 1 μm | ~1 mg $L^{-1}$ | Direct Raman or SERS detection of dry NPs after their homogeneous pre-concentration on glass@PDA or glass@PDA@GNS substrates |

action with PS-NPs. SEM analysis clearly demonstrated that the PDA-mediated preconcentration of small PS-NPs persists even after the incorporation of GNS into the system.

The samples loaded with PS-NPs were carefully washed three times with $ddH_2O$ and dried under nitrogen before proceeding with SERS analysis. As for the other PS-NPs previously analysed, a 225 $\mu m^2$ area was mapped, sampling every 1.5 μm with a 638 nm laser source and a 100× objective. The 638 nm laser source was selected because it provides a better match with the LSPR features of GNS. Average SERS spectra obtained from the map on glass@PDA@GNS substrates loaded respectively with 1 ppm, 2.5 ppm, 5 ppm, 7.5 ppm and 10 ppm of 15 nm PS-NPs are reported in Fig. 7a.

Agreeably, the characteristic peak at 1001 $cm^{-1}$ of the 15 nm PS-NPs is already detectable down to 2.5 ppm, with an increase in the intensity along with the increase in concentration of PS-NPs. In Fig. 7b, the intensities of the 1001 $cm^{-1}$ peak as a function of the concentration of 15 nm PS-NPs are reported. These preliminary results are encouraging, showing how, with simple preparation, combining the adhesive properties of PDA with a SERS-active substrate, it is possible to easily detect PS-NPs down to 15 nm. These findings mark a significant step forward, addressing the persistent challenge of detecting sub-50 nm NPs using SERS.[37]

## 4. Conclusions

In this work, we presented a straightforward approach for NPs detection that exploits a PDA-coating on flat glass substrates. By leveraging the adhesive properties of this biopolymer, we enable the pre-concentration of PS-NPs, facilitating their effective detection *via* Raman and SERS techniques. The influence of pH on the adhesive properties of PDA was evaluated, highlighting the critical role of electrostatic interactions in the grafting process of PS-NPs.

By employing this simple strategy, we successfully achieved the Raman-based detection of PS-NPs of 1 μm and 100 nm size. Additionally, the versatility of the PDA substrate was exploited to immobilize gold nanostars (GNS), producing a SERS-active platform capable of detecting PS-NPs as small as 15 nm at concentrations down to the ppm level. It must be stressed that, even in the latter case, the proposed methodology relies on quite simple substrate preparation. This was accomplished by grafting colloidal GNS onto glass@PDA, once again exploiting the favourable interactions enabled by the biopolymer, which were also harnessed for the further preconcentration of 15 nm PS-NPs.

The Raman- and SERS-based methods proposed so far, even though capable of successfully detecting NPs from aqueous suspensions even at very low concentrations, usually involve complex preparation of the sensing substrate and/or rely on poorly reproducible detection strategies, such as nanoparticle aggregation or dry dropping of NPs suspension (Table 2).[1,36,46–49]

We thus believe that this simple approach will provide valuable insights for the development of reliable Raman- and SERS-based methods for the detection of NPs.

## Author contributions

Serena Schiavi: writing – original draft preparation, formal analysis, investigation, data curation, visualization. Angelo Taglietti: conceptualization, methodology, supervision, project administration, writing – original draft preparation. Pietro Galinetto: writing – review & editing, funding acquisition, supervision, resources. Benedetta Albini: investigation, formal analysis. Om Prakash: formal analysis.

## Conflicts of interest

The authors declare that they have no known competing financial interests or personal relationships that could have appeared to influence the work reported in this paper.

## Data availability

All the data that support the findings of this study have been included within the article and the supplementary information (SI). The authors have ensured that additional details related to the Results and Discussion section are provided in the SI, offering the readers additional figures and tables that can enhance the understanding of the scientific findings. The authors have included supplementary TEM and SEM images of the substrates developed, additional Raman and SERS spectra supporting the experiments referenced in the manuscript as well as additional UV-vis characterizations. Additionally, full details on the EF calculation have been proviided in the SI. See DOI: https://doi.org/10.1039/d5nr02834e.

## Acknowledgements

This research was funded by MIUR, PRIN 2022 project code 2022WAKTFR, "NoveL approaches to mIcro- and nAno-plastIcS detectiOn iN water (LIAISON)". We thank Dr Massimo Boiocchi and Centro Grandi Strumenti (CGS) for TEM measurements. We thank Dr Alessandro Girella and CISRiC Arvedi for SEM measurements.

## References

1 G. Xu, H. Cheng, R. Jones, Y. Feng, K. Gong, K. Li, X. Fang, M. A. Tahir, V. K. Valev and L. Zhang, *Environ. Sci. Technol.*, 2020, **54**, 15594–15603.
2 J. Gigault, H. El Hadri, B. Nguyen, B. Grassl, L. Rowenczyk, N. Tufenkji, S. Feng and M. Wiesner, *Nat. Nanotechnol.*, 2021, **16**, 501–507.
3 M. C. Rillig, *Environ. Sci. Technol.*, 2012, **46**, 6453–6454.
4 Y. Su, X. Hu, H. Tang, K. Lu, H. Li, S. Liu, B. Xing and R. Ji, *Nat. Nanotechnol.*, 2022, **17**, 76–85.
5 S. Luo, J. Zhang and J. C. de Mello, *Front. Bioeng. Biotechnol.*, 2023, **11**, DOI: 10.3389/fbioe.2023.1242797.
6 A. Nene, S. Sadeghzade, S. Viaroli, W. Yang, U. P. Uchenna, A. Kandwal, X. Liu, P. Somani and M. Galluzzi, *Environ. Sci. Eur.*, 2025, **37**, 7.
7 C. M. Rochman, M. A. Browne, B. S. Halpern, B. T. Hentschel, E. Hoh, H. K. Karapanagioti, L. M. Rios-Mendoza, H. Takada, S. Teh and R. C. Thompson, *Nature*, 2013, **494**, 169–171.
8 P. Mishra, S. Vinayagam, K. Duraisamy, S. R. Patil, J. Godbole, A. Mohan, A. Mukherjee and N. Chandrasekaran, *Environ. Sci. Pollut. Res.*, 2019, **26**, 1537–1547.
9 A. Bakir, S. J. Rowland and R. C. Thompson, *Environ. Pollut.*, 2014, **185**, 16–23.
10 Q. Chen, J. Wang, F. Yao, W. Zhang, X. Qi, X. Gao, Y. Liu, J. Wang, M. Zou and P. Liang, *Microchim. Acta*, 2023, **190**, 465.
11 H. Dai, H. Li, W. Qiu, S. Deng, J. Han and T. Aminabhavi, *TrAC, Trends Anal. Chem.*, 2024, **176**, 117750.
12 S. Schiavi, A. Taglietti, A. Magni, P. Galinetto and B. Albini, *Appl. Surf. Sci.*, 2025, **687**, 162223.
13 M. Parmigiani, V. Schifano, A. Taglietti, P. Galinetto and B. Albini, *Nanotechnology*, 2024, **35**, 195603.
14 L. Luan, X. Zhang, P. Li and W. Xu, *Anal. Bioanal. Chem.*, 2025, **417**, 2903–2913.
15 Z. Guo, Y. Zheng, C. Wang, H. Jayan, L. Yin, H. R. El-Seedi, Y. Gong and X. Zou, *Talanta*, 2025, **283**, 127168.
16 W. Zhang, Y. Peng, C. Lin, M. Xu, S. Zhao, D. Li, Y. Yang and Y. Yang, *Chem. Eng. J.*, 2024, **502**, 157907.
17 S. Schiavi, M. Parmigiani, P. Galinetto, B. Albini, A. Taglietti and G. Dacarro, *Appl. Sci.*, 2023, **13**, 9291.
18 S. Kousheh and M. Lin, *Trends Food Sci. Technol.*, 2025, **159**, 104940.
19 X. Lin, F. Lei, X. Liang, Y. Jiao, X. Zhao, Z. Li, C. Zhang and J. Yu, *Opto-Electron. Adv.*, 2025, **8**, 240260–240260.
20 H. Lee, S. M. Dellatore, W. M. Miller and P. B. Messersmith, *Science*, 2007, **318**, 426–430.
21 C.-Y. Liu and C.-J. Huang, *Langmuir*, 2016, **32**, 5019–5028.
22 Y. Li, P. Hu, X. Wang, X. Hou, F. Liu and X. Jiang, *Regener. Biomater.*, 2021, **8**, 1–14.
23 K. Liu, F. Liu and Y. Xu, *Microchim. Acta*, 2025, **192**, 91.
24 H. Zhou, C. C. Mayorga-Martinez and M. Pumera, *Small Methods*, 2021, **5**, 2100230.
25 T. E. Bridges, M. P. Houlne and J. M. Harris, *Anal. Chem.*, 2004, **76**, 576–584.
26 M. Mazilu, A. C. De Luca, A. Riches, C. S. Herrington and K. Dholakia, *Opt. Express*, 2010, **18**, 11382.
27 P. Pallavicini, A. Donà, A. Casu, G. Chirico, M. Collini, G. Dacarro, A. Falqui, C. Milanese, L. Sironi and A. Taglietti, *Chem. Commun.*, 2013, **49**, 6265.
28 J. Guthmuller and B. Champagne, *J. Phys. Chem. A*, 2008, **112**, 3215–3223.
29 C. Wu, E. Chen and J. Wei, *Colloids Surf. A Physicochem. Eng. Asp.*, 2016, **506**, 450–456.
30 V. Ball, D. Del Frari, V. Toniazzo and D. Ruch, *J. Colloid Interface Sci.*, 2012, **386**, 366–372.
31 D. Bogdan, I.-G. Grosu and C. Filip, *Appl. Surf. Sci.*, 2022, **597**, 153680.
32 V. Ball, *Colloids Surf. A Physicochem. Eng. Asp.*, 2010, **363**, 92–97.
33 M. Duan, Q. Tang, M. Wang, M. Luo, S. Fang, X. Wang, P. Shi and Y. Xiong, *Water Sci. Technol.*, 2020, **82**, 2353–2365.
34 L. Ghidoni, S. Schiavi, P. Pallavicini, L. Doveri, Y. A. D. Fernandez, A. Taglietti and G. Dacarro, *Colloids Surf. A Physicochem. Eng. Asp.*, 2025, **727**, 138460.
35 M. L. Alfieri, T. Weil, D. Y. W. Ng and V. Ball, *Adv. Colloid Interface Sci.*, 2022, **305**, 102689.
36 B. Chaisrikhwun, S. Ekgasit and P. Pienpinijtham, *J. Hazard. Mater.*, 2023, **442**, 130046.
37 D. Mrđenović, D. Abbott, V. Mougel, W. Su, N. Kumar and R. Zenobi, *ACS Appl. Mater. Interfaces*, 2022, **14**, 24938–24945.

 

38 X. Xu, *Opt. Commun.*, 2001, **199**, 89–93.
39 M. B. Mohamed, V. Volkov, S. Link and M. A. El-Sayed, *Chem. Phys. Lett.*, 2000, **317**, 517–523.
40 F. Talamona, M. Truffi, A. A. Caldarone, A. Ricciardi, F. Corsi, G. Pellegrini, C. Morasso and A. Taglietti, *Nanotechnology*, 2021, **32**, 295703.
41 F. Le, D. W. Brandl, Y. A. Urzhumov, H. Wang, J. Kundu, N. J. Halas, J. Aizpurua and P. Nordlander, *ACS Nano*, 2008, **2**, 707–718.
42 R. Boyack and E. C. Le Ru, *Phys. Chem. Chem. Phys.*, 2009, **11**, 7398.
43 M. Parmigiani, B. Albini, G. Pellegrini, M. Genovesi, L. De Vita, P. Pallavicini, G. Dacarro, P. Galinetto and A. Taglietti, *Nanomaterials*, 2022, **12**, 3609.
44 Z. Li and H. Xu, *Adv. Phys. X*, 2016, **1**, 492–521.
45 B. Albini, M. Parmigiani, G. Pellegrini, A. Taglietti and P. Galinetto, *J. Mater. Sci.: Mater. Electron.*, 2023, **34**, 1619.
46 L. Lv, L. He, S. Jiang, J. Chen, C. Zhou, J. Qu, Y. Lu, P. Hong, S. Sun and C. Li, *Sci. Total Environ.*, 2020, **728**, 138449.
47 L. Mikac, I. Rigó, L. Himics, A. Tolić, M. Ivanda and M. Veres, *Appl. Surf. Sci.*, 2023, **608**, 155239, DOI: 10.1016/j.apsusc.2022.155239.
48 J. Caldwell, P. Taladriz-Blanco, B. Rothen-Rutishauser and A. Petri-Fink, *Nanomaterials*, 2021, **11**, 1149.
49 Y. Liu, L. Lin, B. Yang, M. Huang, X. Huang, X. Chen, Z. Dai, S. Sun, Y. Yang and C. Li, *ACS Sustainable Chem. Eng.*, 2024, **12**, 1595–1604.